doi:10.1016/j.jmb.2007.09.048 J. Mol. Biol. (2007) 374, 517–527

JMB

Available online at www.sciencedirect.com

ScienceDirect

ELSEVIER

A 1.3-Å Structure of Zinc-bound N-terminal Domain of Calmodulin Elucidates Potential Early Ion-binding Step

Julia T. Warren[1]†, Qing Guo[2]† and Wei-Jen Tang[1,2]*

[1]*Biological Sciences Collegial Division, The University of Chicago, Chicago, IL 60637 USA*

[2]*Ben-May Department for Cancer Research, The University of Chicago Chicago, IL 60637, USA*

Received 9 June 2007; received in revised form 13 September 2007; accepted 18 September 2007
Available online
21 September 2007

Calmodulin (CaM) is a 16.8-kDa calcium-binding protein involved in calcium-signal transduction. It is the canonical member of the EF-hand family of proteins, which are characterized by a helix–loop–helix calcium-binding motif. CaM is composed of N- and C-terminal globular domains (N-CaM and C-CaM), and within each domain there are two EF-hand motifs. Upon binding calcium, CaM undergoes a significant, global conformational change involving reorientation of the four helix bundles in each of its two domains. This conformational change upon ion binding is a key component of the signal transduction and regulatory roles of CaM, yet the precise nature of this transition is still unclear. Here, we present a 1.3-Å structure of zinc-bound N-terminal calmodulin (N-CaM) solved by single-wavelength anomalous diffraction phasing of a selenomethionyl N-CaM. Our zinc-bound N-CaM structure differs from previously reported CaM structures and resembles calcium-free apo-calmodulin (apo-CaM), despite the zinc binding to both EF-hand motifs. Structural comparison with calcium-free apo-CaM, calcium-loaded CaM, and a cross-linked calcium-loaded CaM suggests that our zinc-bound N-CaM reveals an intermediate step in the initiation of metal ion binding at the first EF-hand motif. Our data also suggest that metal ion coordination by two key residues in the first metal-binding site represents an initial step in the conformational transition induced by metal binding. This is followed by reordering of the N-terminal region of the helix exiting from this first binding loop. This conformational switch should be incorporated into models of either stepwise conformational transition or flexible, dynamic energetic state sampling-based transition.

Keywords: calmodulin; EF-hand motif; metal ion binding; metal ion induced conformational switch; X-ray crystallography

Edited by R. Huber

Introduction

The complex processes of intracellular calcium ion (Ca^{2+}) signaling rely heavily on members of the EF-hand protein family for signal transduction and regulation.[1] These proteins contain a helix–loop–helix calcium-binding EF-hand motif and most undergo a substantial conformational change upon binding calcium. Examples of this transition between Ca^{2+}-free (apo) and Ca^{2+}-loaded EF-hands include calmodulin (CaM), troponin C, and members of the S100 family.[2] CaM, a highly conserved 148-amino-acid protein, has been extensively studied due to its ability to bind to and modulate a large number of target proteins, in conjunction with its involvement in signal transduction of Ca^{2+} signals. The ubiquitous involvement of CaM in such a diversity of cellular processes is thought to stem from its ability to sense Ca^{2+} with a range of affinities that correlate to intracellular Ca^{2+} levels in most cells ($K_d = 5\times10^{-7}$ to 5×10^{-6} M).[3–5] It is able to selectively bind Ca^{2+} despite the fact that in the resting cell, there are high levels of other cations, especially the divalent magnesium cation (Mg^{2+}), which is present in concentrations between 0.4 and 1 mM (roughly 100- to 10,000-fold higher than intracellular Ca^{2+} concentrations). CaM also uses

*Corresponding author. E-mail address: wtang@uchicago.edu.

† Both authors contributed equally to this work.

Abbreviations used: CaM, calmodulin; N-CaM, N-terminal calmodulin; C-CaM, C-terminal calmodulin.

many different binding modes to interact with its sequence- and structure-diverse targets.[6] Such binding could lead to the activation of its effectors by mechanisms of the removal of autoinhibition, dimerization, or catalytic site rearrangement.[7]

Extensive studies both by X-ray crystallography and by NMR[8–10] have revealed the conformational switch from apo-CaM to Ca^{2+}-loaded CaM in atomic detail. CaM possesses two globular N- and C-terminal domains, termed N- and C-CaM, that each contain two EF-hand motifs.[11,12] A four-helix bundle in N-CaM is tethered to a four-helix bundle in C-CaM by a flexible linker. Ca^{2+} binding occurs in the loop region of all four EF-hand motifs. Each Ca^{2+} is coordinated by the side-chain oxygen atoms of four residues in the DXDXD/NXXXXXXE consensus sequence and one main-chain carbonyl oxygen from the residue at the seventh position. Upon Ca^{2+} binding, CaM undergoes a large conformational change involving reorientation of the helices in each domain. The coordinated movement of the two EF-hand motifs in N- and C-CaM triggers the conformational switch from a compact "closed" state to an "open" conformation, in the process exposing a large hydrophobic pocket.[13] This hydrophobic pocket, rich in methionines, is thought to contribute to CaM's sequence-independent recognition of target proteins.

However, the structural details for the transition from apo-CaM to Ca^{2+}-loaded CaM remain unclear. The importance of this structural transition has been emphasized across the EF-hand protein family regarding its role in target recognition and calcium signal transduction. Discussion of this structural transition in CaM has centered around highly specific, stepwise transitions[14] or models where apo-CaM samples a flexible, dynamic range of conformations at specific sites.[13,15] The interaction of zinc ion (Zn^{2+}) with CaM has several unique properties. While Zn^{2+} binds CaM, it does not induce the global conformational change of CaM.[16] Here, we report a zinc-bound N-CaM structure at 1.3-Å resolution. The comparison with apo-CaM, Ca^{2+}-loaded CaM in its open conformation, and Ca^{2+}-loaded CaM in its closed conformation suggests that our structure may represent an early intermediate step in the metal binding and may provide new structural insights into the transition between apo-CaM and Ca^{2+}-loaded CaM.

Results and Discussion

Structural determination of N-CaM

Bordetella pertussis, the etiologic agent of whooping cough, secretes a CaM-activated adenylyl cyclase toxin named CyaA. Both N-CaM and C-CaM can potently activate the catalytic activity of this toxin. We have solved the structure of the C-CaM-bound adenylyl cyclase domain of CyaA, providing structural insight into the molecular basis of CaM-mediated toxin activation.[17] However, the structural basis by which N-CaM is able to contribute to a 400-fold increase in activation remains elusive. An attempt to crystallize N-CaM-bound CyaA yielded instead a crystal containing N-CaM alone, which diffracted to 2.0 Å resolution. The lack of a CyaA/N-CaM complex was suspected by the small size of the unit cell and confirmed by SDS-PAGE analysis of a dissolved crystal. Efforts to solve this structure using molecular replacement with both Phaser and AMoRe[18] and using multiple search models (1J7O,[13] 1UP5,[19] CFC,[9] and 1F54[20]) failed. We therefore suspected the presence of a previously unreported conformation and proceeded to use selenomethionyl N-CaM to obtain experimental phases through the technique of single-wavelength anomalous diffraction.

Crystals of selenomethionyl N-CaM grew at 4 °C in a solution containing 16% PEG8000, 100 mM sodium cacodylate (pH 6.3) and 5 mM $ZnCl_2$. Crystals diffracted to 1.3 Å and formed a tetragonal lattice with space group $P4_32_12$ containing a single molecule in the asymmetric unit. Refinement was performed with Refmac followed by anisotropic thermal displacement factors using Shelx97. Final data statistics of the model converged at R_{work} = 14.2%, R_{free} = 19.6% and are listed in Table 1.

We observe clear electron density for residues 2–76 (Fig. 1a), which includes the two helix–loop–helix motifs expected for N-CaM (Fig. 1b). Two Zn^{2+} ions as well as a cacodylate molecule, which is involved in Zn^{2+} coordination, are found in this structure (Fig. 1b). The identity of these two Zn^{2+} ions and arsenic atom of cacodylate was confirmed by strong anomalous signals from data collected at both the zinc (Fig. 2a) and arsenic edges (Fig. 2b). The crystal packing is unusual for a CaM structure. Briefly, along one axis, molecules of N-CaM are arranged in a head-to-head fashion in the crystal lattice such that the first ion-binding site has direct symmetry contact with its corresponding site in the symmetry-related molecule (Fig. 2c). This allows cacodylate to coordinate two Zn^{2+} ions from the first EF hand motif within two symmetry-related partners.

Noting that Ca^{2+} is the most commonly cited metal ion ligand of CaM, we attempted to soak in Ca^{2+} during the crystallization process. However, high concentrations of $CaCl_2$ (100 mM) caused the crystal to shatter. We therefore gradually reduced the Ca^{2+} to a concentration that allowed us to preserve the N-CaM crystal (5 mM $CaCl_2$) and collected data that diffracted to 1.6 Å (Table 1). We then determined this structure and found it to be nearly identical with the non-Ca^{2+}-soaked crystal structure. Interestingly, using the fast Fourier transform operation in the Crystallography and NMR System (CNS)[21] software suite to generate anomalous difference maps from signals collected at the zinc and arsenic edges, we found similar ligand occupation ratios in the non-Ca^{2+}-soaked and Ca^{2+}-soaked crystals (Supplementary Fig. 1). We concluded that this structure still contained Zn^{2+}, and therefore from here on, we will use only the non-Ca^{2+}-soaked version of N-CaM for our structural analysis.

Table 1. Crystallographic statistics

	Se N-CaM	Native N-CaM	Native N-CaM (Ca2+-soaked)	Zn N-CaM	As N-CaM
Data collection					
Beam line	APS 19-ID	APS 19-BMC	APS 19-ID	APS 19-BMC	APS 19-BMC
Wavelength (Å)	0.97929	0.97951	0.97929	1.28237	1.04393
Space group	$P4_32_12$	$P4_32_12$	$P4_32_12$	$P4_32_12$	$P4_32_12$
Cell dimension (Å)					
a	35.2	35.3	35.2	35.3	35.1
b	35.2	35.3	35.2	35.3	35.1
c	142.6	143.2	143.3	142.5	143.3
Resolution (Å)	50–2.0	32–1.3	30–1.6	50–2.2	50–2.2
R_{sym} (%)[a]	12.4 (36.2)	7.0 (31.5)[b]	7.6 (48.5)[b]	16.3 (25.3)	14.5 (29.8)
I/sigma	41.2 (10.1)	46.1 (3.8)[b]	27.2 (3.2)[b]	45.8 (12.0)	47.5 (15.7)
Redundancy[c]	29.3 (30.1)	12.5 (8.6)[b]	13.2 (9.1)[b]	24.6 (26.2)	23.6 (25.0)
Completeness (%)	98.3 (97.8)	99.0 (92.1)[b]	99.8 (99.4)[b]	99.9 (99.9)	99.9 (99.9)
Figure of merit	0.87				
Unique reflections	36,347	12,687	12,125	33,915	32,184
Refinement					
R_{work}[d]		0.142	0.174		
R_{free}[e]		0.196	0.215		
No. atoms					
Protein		612	612		
Water		126	117		
B-factors					
Protein		9.5	9.6		
Water		10.9	11.2		
r. m. s. deviations					
Bond lengths (Å)		0.008	0.009		
Bond angles (°)		1.17	1.21		
Ramachandran plot (%)					
Favorable region		95.4	95.4		
Allowed region		4.6	4.6		
Generously allowed region		0	0		
Disallowed region		0	0		

[a] $R_{sym} = \sum_j | <I> - I_j | / \sum <I>$ where I_j is the intensity of the *j*th reflection and $<I>$ is the average intensity.
[b] The outer resolution shell.
[c] N_{obs}/N_{unique}.
[d] $R_{work} = \sum_{hkl} | F_{obs} - F_{calc} | / \sum_{hkl} F_{obs}$.
[e] R_{free}, calculated the same as for R_{work} but on the 5% data excluded from the refinement calculation.

Structural characterization of zinc-bound N-terminal domain of CaM

The overall structure of N-CaM is composed of a four-helix bundle making internal contacts as well as contacts with symmetry-related molecules (Figs. 1b and 2c). The first Zn^{2+} ion is tetrahedrally coordinated by two aspartate residues (Asp22 and Asp24 of the first calcium-binding loop), which are known to coordinate Ca^{2+} in the Ca^{2+}-loaded CaM structure,[22] and by two cacodylate molecules, the arsenic buffer used in the crystallization conditions. There is also one highly ordered water molecule (sigma >6.0 in the $F_o - F_c$ map) in site 1 coordinated by several residues normally involved in metal ion binding (Thr26 and Asp20 of the first calcium-binding loop). The second Zn^{2+} ion is also tetrahedrally coordinated by residues Glu67 (normally involved in coordination) and Asp64 of N-CaM as well as by two residues (Glu7 and Glu11) of the symmetry-related molecule (Fig. 2c). Thus, four of five residues of the second calcium-binding loop normally involved in calcium binding are not liganded to the second zinc ion. This Zn^{2+} ion also shows significant anisotropy and is best modeled as one Zn^{2+} ion with multiple occupancy (Fig. 1b).

Within both EF-hand domains, the integrity of the helical secondary structure is intact, noting that there is a slight deviation from α-helical structure in the N-terminal region of helix B. The two metal-binding loops are largely in the unliganded conformation, with three of five residues from binding site 1 and four of five from binding site 2 not actively coordinating metal due to large distance and orientational constraints. Between these pair-mate EF-hands, there is a region containing four hydrogen bonds maintained between the backbone carbonyl groups and nitrogen atoms of residues Gly25-Phe65, Ile27-Thr63 (CO–N and N–CO), and Thr29-Gly61. The importance of this region in a Ca^{2+}-induced conformational change was proposed as acting to stabilize the calcium-free, compact helix form while allowing a relative rigid structure around which helices B/C rotate during domain opening.[14]

Structural comparison of zinc-bound N-CaM with ion-free and calcium-loaded structures

To determine how similar our structure is to other previously reported CaM structures, we first

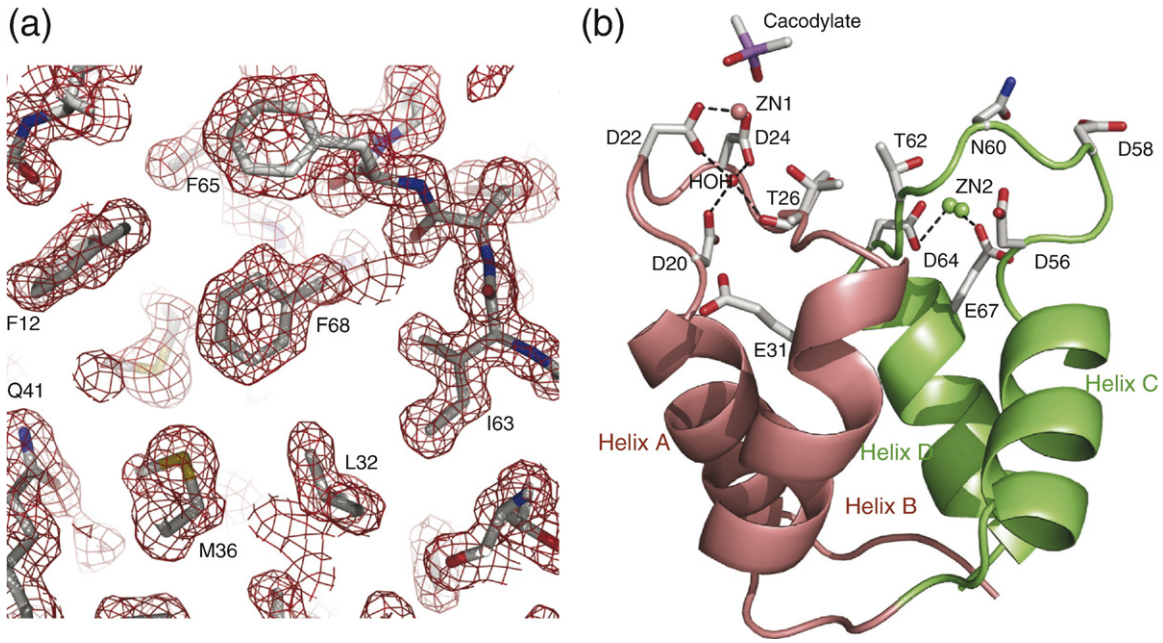

Fig. 1. The overall structure of zinc-bound N-CaM. (a) The $2F_o - F_c$ density map of N-CaM contoured at 1.2 σ. (b) The ribbon representation of N-CaM. The two helix–loop–helix EF-hand Zn^{2+} binding sites are shown in different colors: EF-hand I (helices A and B), rose red; EF-hand II (helices C and D), lime green. The spheres show the two Zn^{2+} ions present in these binding sites. The zinc ion in site 2 has double occupancy. There is also a cacodylate molecule present from the crystal growth buffer with arsenic shown in purple. The side chains of the residues involved in binding are shown in stick representation with different colors: carbon, gray; nitrogen, blue; oxygen, red. Residue T26 shows alternative conformation.

performed structural alignments using each of the individual helices (A–D) and then helices A and D together (residues 6–18 and 65–74, respectively) or B and C together (residues 29–38 and 45–54) followed by calculating RMSD values. The Zn^{2+}-bound N-CaM structure is globally similar to the NMR structure of the Ca^{2+}-free CaM (C^{α} RMSD = 0.929 Å for residues 4–76, 1CFD[9]), the X-ray crystallographic structure of the Ca^{2+}-free N-domain of CaM alone (C^{α} RMSD = 0.62 Å, 1QX5[8]) and of 41/75 cross-linked CaM (C^{α} RMSD = 1.161 Å, 1Y6W[14]). These low RMSD values indicate that our structure is indeed in a state most closely resembling the native Ca^{2+}-free conformation (Table 2). It is expected that within individual helices there is not substantially large reorientation between closed and open states, and on the level of the individual helix our structure is similar to the calcium-loaded structure with the exception of helix B, where there appears to be significant structural difference (C^{α} RMSD = 1.159 Å). A larger RMSD is expected for the anti-parallel β-sheet region due to the fact that different numbers of hydrogen bond pairs are possible in the closed *versus* open conformations (C^{α} RMSD = 0.434 Å, 1CFD, and C^{α} RMSD = 0.932 Å, 1CLL).

The similarity of our Zn^{2+}-bound N-CaM structure to the ligand-free CaM is clearly revealed by the superposition of our structure (opaque) and the Ca^{2+}-free CaM (1CFD) and Ca^{2+}-loaded CaM (1CLL) structures (transparent) (Fig. 3). The closed conformation of this Zn^{2+}-bound N-CaM structure can be further confirmed by comparing the interhelical angles calculated for several high-resolution structures using the program Interhlx (Kyoko Yap, University of Toronto). Again, structural alignments were performed using a combination of helices A and D together (residues 6–18 and 65–74). Theoretical lines can be drawn through each helix, and the calculation of angles between these lines provides an interhelical angle. In addition, we calculated a theoretical center of mass for each helix and found the distances between these centers of mass as another measure of global similarity between structures. Generally speaking, the conformational change that moves CaM from a closed form to an open form involves the "swinging" of helices B and C away from helices A and D. Examining the interhelical angles between helices A/B, A/C, or C/D provides the most obvious examples of this helical movement and values calculated for the structure presented here resemble strongly the closed conformation (Table 3).

Zn^{2+}-coordination sites

There are two ion-binding sites in the two EF-hands of N-CaM. Anomalous data collected at the Zn edge confirm that these two sites are occupied by Zn^{2+} (Fig. 2a). While these are the same two binding sites as are found in other ion-bound structures of CaM, the ways in which they coordinate the ions differ from previously reported structures. The coordination of Zn^{2+} in binding site 1 is different from that of previously reported Ca^{2+}-coordinating structures. Here, only two residues (Asp22 and Asp24) coordinate the metal ion, while

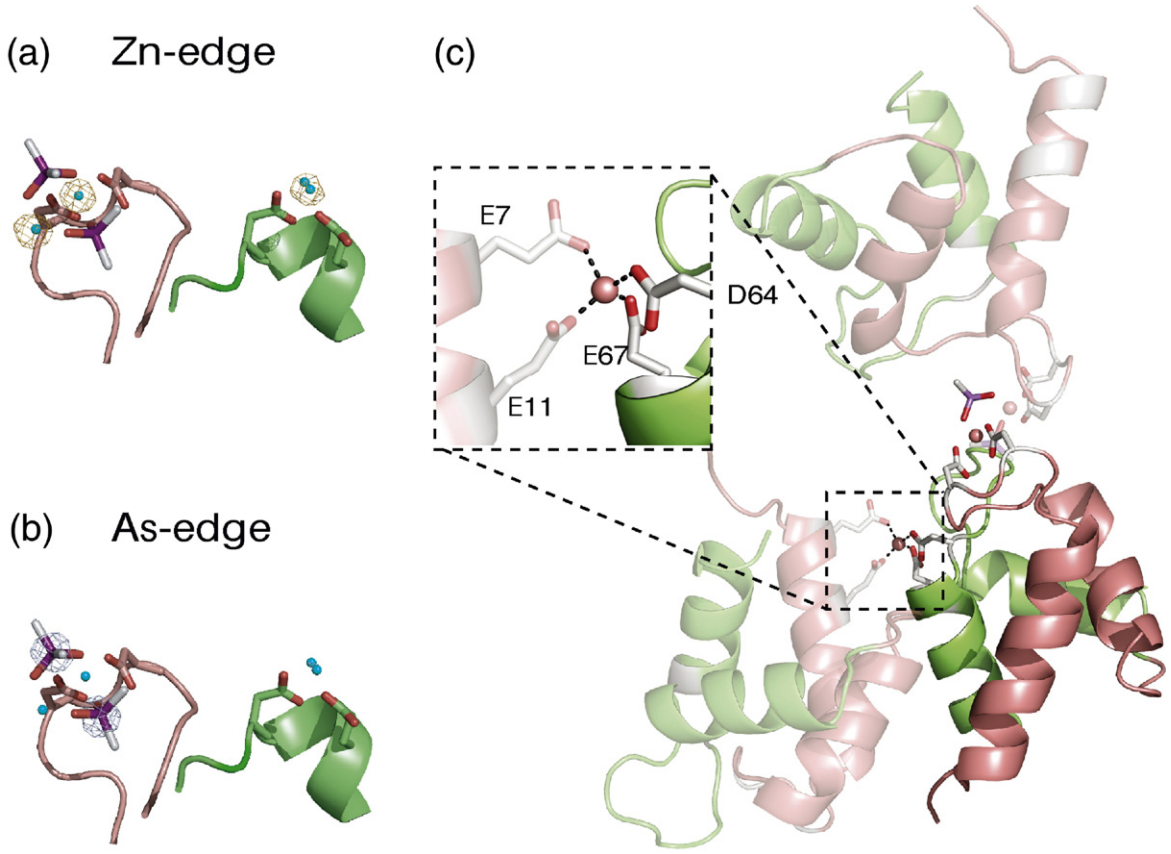

Fig. 2. Structural details in the metal-binding sites, ligand identity, and molecular packing. (a) $2F_o - F_c$ map calculated from data collected at the zinc edge (λ = 1.28237 Å). (b) $2F_o - F_c$ map calculated from data collected at the arsenic edge (λ = 1.04393 Å). (c) Molecule packing in the asymmetric unit of N-CaM. Transparent molecules are symmetry-related molecules. The two helix–loop–helix EF-hand Zn^{2+}-binding sites are shown in different colors: EF-hand I (helices A and B), rose red; EF-hand II (helices C and D), lime green. The spheres show the two Zn^{2+} ions present in these binding sites. The zinc ion in site 2 has double occupancy. There is also a cacodylate molecule present from the crystal growth buffer with arsenic shown in purple. The side chains of the residues involving the binding are shown in stick representation with different colors: carbon, gray; nitrogen, blue; oxygen, red.

the other three normally involved in metal coordination are greater than 4 Å away. In particular, Glu31 (the most C-terminal residue of the binding loop) is roughly 10 Å away from the Zn^{2+} ion. This is significant because the glutamate at this position has been shown to be necessary for Ca^{2+} binding through mutational studies,[23] and its importance in the mechanism of Ca^{2+} binding was recently outlined.[14] In fact, replacement of Glu31 in any of the sites in CaM causes a dramatic decrease in Ca^{2+} affinity and impairs the conformational change.[24,25] Because the coordination of our second Zn^{2+} ion involves three of four residues typically not implicated as being important for Ca^{2+} binding (Asp 64 and Glu7, Glu11 of the symmetry-related molecule), we conclude that its presence here is to facilitate the crystal packing between two N-CaM molecules. A previous flow dialysis study revealed

Table 2. Comparison of the N-CaM with apo and Ca^{2+}-bound structures of CaM

	Segment[b]							
Protein[a]	N-CaM	Helix A	Helix B	Helix C	Helix D	Helices A+D	Helices B+C	EF-hands scaffold
Apo-CaM	0.929	0.324	0.299	0.295	0.363	0.598	0.452	0.434
Ca^{2+}-loaded CaM	4.512	0.561	1.159	0.297	0.273	1.474	0.276	0.932
CaM 45/71	1.161	0.302	0.735	0.440	0.200	0.545	0.950	0.454

[a] Accession numbers for Apo-CaM, calcium-loaded CaM, and calcium-loaded cross-linked CaM 41/75 are 1CFD, 1CLL, and 1Y6W, respectively.

[b] Definition of helices in CaM: helix A (aa 6–18), helix B (aa 29–38), helix C (aa 45–54), helix D (aa 65–74). N-CaM includes amino acid residues 4–76 and the EF-hand β-sheet scaffold includes amino acid residues 25–27 and 61–63. The C^{α} RMSD values are listed for the alignment of various segments. For the EF hand β-sheet scaffold, all backbone atoms are used for the alignment. Values for RMSD were obtained from the align function of the program Coot.

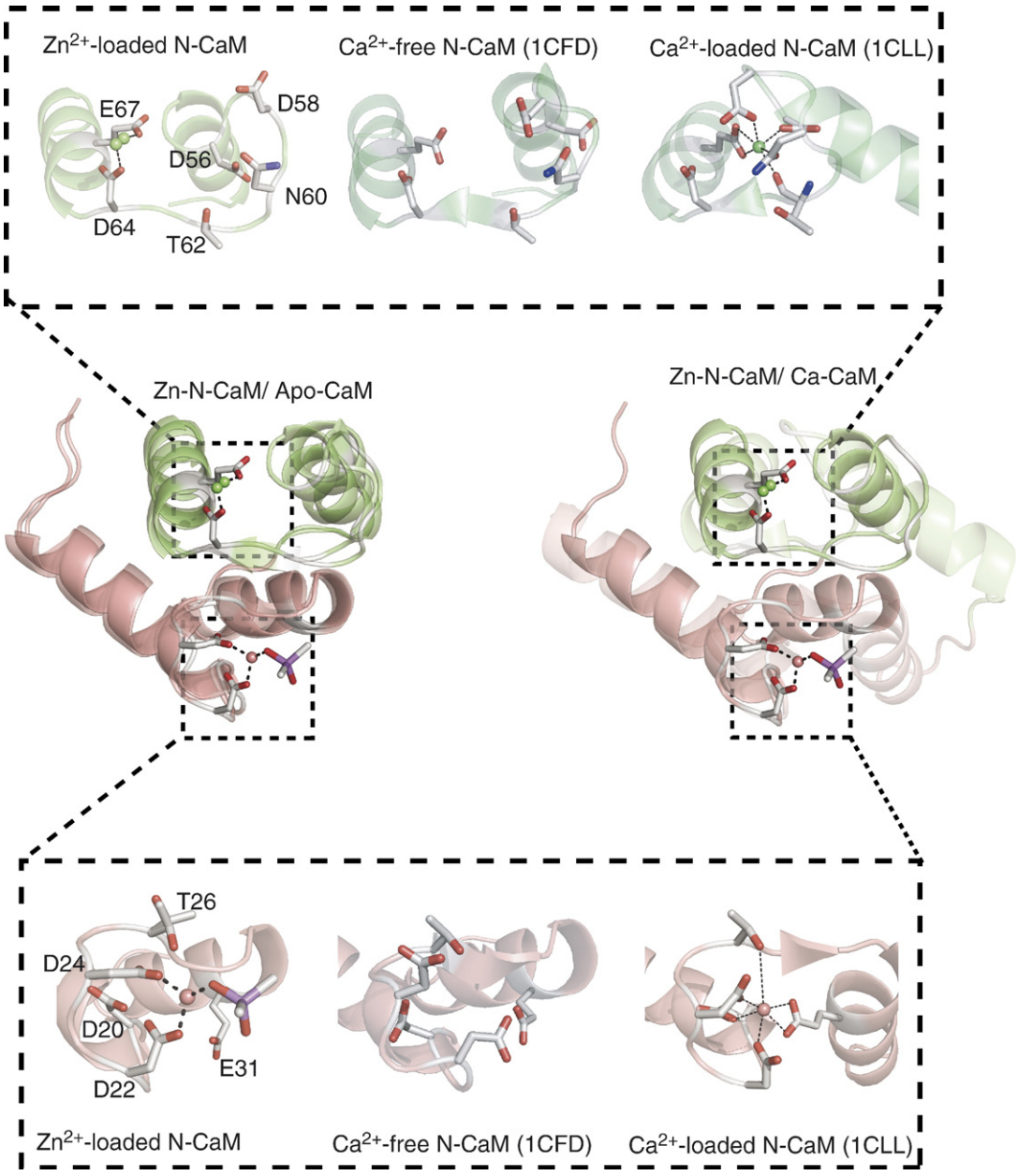

Fig. 3. Structure alignment of N-CaM with N-terminal domain of the NMR structure of apo-CaM (left, 1CFD) and the X-ray structure of Ca^{2+}-CaM (right, 1CLL). The residues involved in ion coordination are shown as sticks and labeled. These global alignments were performed using helices A and D, and show that our structure is predominantly in the closed conformation. 1CFD and 1CLL are presented as transparent. The two helix–loop–helix EF-hand Zn^{2+}-binding sites are shown in different colors: EF-hand I (helices A and B), rose red; EF-hand II (helices C and D), lime green. The spheres show the two Zn^{2+} ions present in these binding sites. The zinc ion in site 2 has double occupancy. There is also a cacodylate molecule present from the crystal growth buffer with arsenic shown in purple.

that CaM has two Zn^{2+} ion sites with 80–300 μM affinity as well as four or five lower affinity Zn^{2+}-binding sites.[26] It is possible that the Zn^{2+} ion revealed by our N-CaM structure is one of those low-affinity sites whose precise positions have not previously been identified.

Effect of Zn^{2+} ion on the activation of bacterial adenylyl cyclase toxins by CaM

Zn^{2+} has been shown to be capable of supporting the activation of the CaM effector myosin light-chain kinase by CaM (roughly 18% above baseline), although such activation is significantly less than the activation by other ions such as cadmium (Cd), terbium (Tb), and europium (Eu).[27] Consistent with this observation, although Cd, Tb, and Eu can induce a measurable global conformational change in CaM based on based on Fourier-transform infrared spectroscopy and electron-spin spectroscopy studies. Zn^{2+} ion affects the activation of CaM effectors, we examined the effect of Zn^{2+} ion on the activation of anthrax edema factor (EF) and pertussis CyaA by CaM (Fig. 4).

Table 3. Spatial relation between α-helices in CaM

Protein[a]	Helices[b]					
	A–B	A–C	A–D	B–C	B–D	C–D
N-CaM	133 (12.6)[c]	−84 (17.6)	133 (10.8)	113 (8.6)	−46 (13.3)	143 (12.0)
Apo-CaM	136 (12.9)	−93 (21.2)	126 (10.6)	124 (11.9)	−49 (12.9)	129 (14.1)
CaM 41/75	129 (13.4)	−97 (21.4)	129 (10.7)	122 (12.6)	−50 (12.6)	127 (13.0)
Ca^{2+}-loaded CaM	88 (18.9)	−161 (22.8)	107 (10.5)	112 (11.2)	−41 (18.0)	87 (16.2)

[a] Accession numbers for zinc-bound N-CaM, Apo-CaM, calcium-loaded CaM, and calcium-loaded cross-linked CaM 41/75 are 2PQ3, 1CFD, 1CLL, and 1Y6W, respectively.
[b] Definition of helices in CaM: helix A (aa 6–18), helix B (aa 29–38), helix C (aa 45–54), helix D (aa 65–74).
[c] The interhelical angles (degrees) and distances (Å) between centers of mass (in parentheses). These were calculated with the program Interhlx. The angles are defined as described by Drohat *et al.*[47] as follows: (1) the molecule is oriented in such a way that the helices of interest (*i*,*j*) are in planes parallel with the screen; (2) the first helix (*i*) is in front of the second helix (*j*), and the first helix (*i*) is aligned vertically (0°) with its N→C vector pointing upward. An imaginary vector aligned vertically (0°) with its tail at the N terminus of the second helix (*j*) is rotated (by ≤180°) clockwise or counterclockwise until it is aligned with the N→C vector of the second helix (*j*). This angle of rotation defines the interhelical angle Ω with a clockwise rotation giving a positive Ω value and a counterclockwise rotation giving a negative Ω value.

EF and CyaA are bacterial toxins secreted by pathogenic bacteria that cause anthrax and pertussis, respectively. While both toxins have CaM-activated adenylyl cyclase activity to intoxicate the target cells by raising the intracellular cAMP level, their binding to CaM differs substantially.[17,28,29] We found that in the presence of 10 mM Zn^{2+}, CaM could activate EF but not CyaA. However, the V_{max} for the adenylyl cyclase activity of CaM-activated EF in the presence of $Zn^{2+}$is approximately 10-fold lower than that in the presence of 1 μM free Ca^{2+}. Together, these data indicate that Zn^{2+} ion is capable of partially substituting the ability of Ca^{2+} to modulate the activity of CaM effectors such as myosin light-chain kinase and anthrax EF. These data further suggest that Zn^{2+}-bound CaM is partially able to activate its effectors and may represent a conformational intermediate between apo-CaM and Ca^{2+}-loaded CaM.

Mechanistic aspects of the early stages of metal ion binding

The Ca^{2+}-binding loop of CaM is 12 residues in length and several key residues are highly conserved across EF-hand Ca^{2+}-binding proteins. In CaM, the loop (N-terminal residue) begins with an aspartate residue and ends with a glutamate residue, both of which coordinate Ca^{2+}. In between, three other highly conserved residues are involved in coordination: the side-chain carboxylic acids of two aspartates and the main-chain carbonyl oxygen of a threonine residue. The NMR structures of apo-CaM and crystallographic temperature factors appear to show a more dynamic N-terminal of the loop region, while the C-terminal part of the loop is highly structured. This is due to main-chain hydrogen bonds of an anti-parallel β-sheet (contacts between residue 25 and 65, 27 and 63, as well as 29 and 61) in apo-CaM, which significantly constrains the flexibility of the C-terminal part of the Ca^{2+}-binding loops of the pair-mate EF-hand.[30]

In our structure, the residues immediately C-terminal to this region (residues 28–33) maintain a non-α-helical secondary structure, and are more consistent with the hydrogen bond patterns of a 3_{10}-helix (Fig. 5). This pattern is also seen in NMR and X-ray structures of apo-CaM;[9,20] however, this is missing from a recently reported cross-linked CaM (41/75) trapped intermediate structure.[14,16] These residues

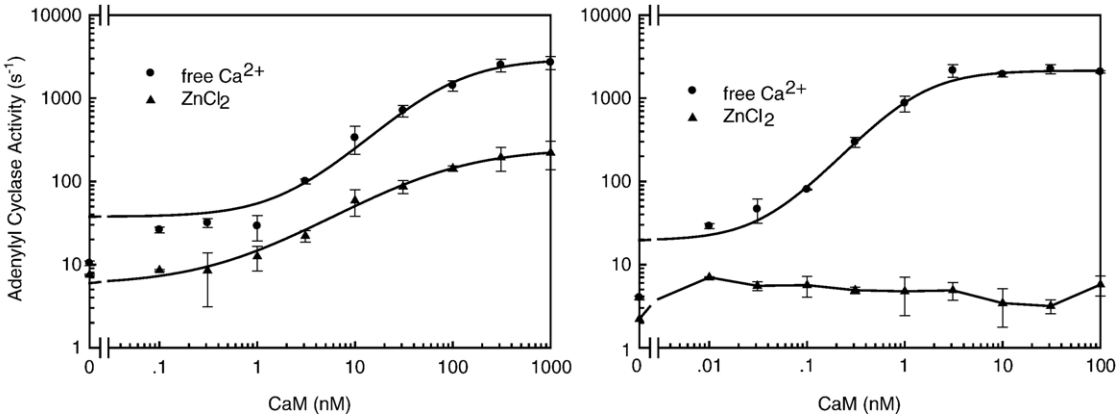

Fig. 4. The effect of zinc ion on the activation of two bacterial adenylyl cyclase toxins, EF and CyaA, by CaM. Assays were performed at 30 °C for 10 min in the presence of 1 nM EF or CyaA with the indicated concentration of CaM either with 10 mM $ZnCl_2$ or 1 μM free calcium ion buffered by EGTA; data are a representative of two experiments.

adopt the typical i, $i+4$ hydrogen bonding patterns observed in α-helices in the Ca^{2+}-loaded, open conformation structures.[20,22] It follows that in order to adopt the α-helical, rigid position of these residues, which is present in the Ca^{2+}-loaded structures, these residues would need to undergo significant reordering of the main-chain atoms in concert with movement of the bidentate Glu31 into a coordinating position. In the cross-linked intermediate CaM mechanism discussion, this helical region simply moves into a position where this bidentate Glu31 is able to complete Ca^{2+} coordination. There is no discussion of required helical reordering, possibly due to the fact that trapping this state with a cross-linking disulfide bond created an α-helical structure that is not necessarily present in the initial stages of metal ion binding.

The structural comparison with apo- and Ca^{2+}-loaded CaM leads to the hypothesis that our structure might represent a trapped intermediate binding state. We propose that metal ion coordination may begin with several N-terminal loop region aspartates, and that initially the ligand site is occupied by a highly coordinated water molecule (sigma >6.0 in $1F_o-F_c$). In order for full metal ion coordination to occur, several steps must take place: the coordinated water molecule must be displaced. To do so, there must be reordering and, therefore, flexibility of the region immediately C-terminal to the binding loop. In addition, the remaining aspartate, carbonyl main-chain oxygen, and bidentate glutamate must also move into position. In our Zn^{2+}-bound N-CaM structure, the metal ion in binding site 1 is coordinated by only two aspartate residues, leaving the possibility that this represents one of the first steps in metal ion coordination. Here, these two residues would be able to maintain first contacts with the metal ion, followed by neighboring side chains of Asp20 and main-chain carbonyl of Thr26. The highly ordered water molecule, which in our structure makes contacts with the main-chain carbonyl of Thr26, must be displaced before coordination between these four residues together could take place. In addition, the main-chain residues 28–33 of the N terminus of the exiting helix need to rearrange to an α-helical orientation in conjunction with the movement of Glu31 into a coordinating position.

While we describe these conformational changes in a discrete, stepwise manner, it is also possible that the intermediate we have trapped represents one of the energy states that the N-terminal domain may sample between the canonical closed and open conformations. Consistent with lower temperature factors and less flexibility in NMR data of the C-terminal region after the binding loop, this suggests that reordering of this region may happen only after binding of a metal ion by more than two of the four N-terminal coordinating residues. This would explain why the N-terminal region of helix B, which is located at the C-terminal region of the first binding loop, maintains the 3_{10}-helical structure, although we do see coordination of a metal ion by two of five residues at the first binding loop. In a recently reported structure of a trapped intermediate formed by a cross-linking disulfide bond between residues 41/75, the author suggests that exiting helix B pivots around residue Ile27 in a locked, α-helical form as a step in the conformational switch. In this manner, reordering of this region and movement of Glu31 into a coordinating position could then cause the observed "swinging" of helices B/C relative to A/D that takes place during the conformational change. Our structure implies an earlier stage during which this α-helical region has not yet formed, and therefore our structure may represent an earlier step in metal ion binding that is a prerequisite for helical reordering and movement. Taken together, these steps describe the potential mechanism by which the motion of the

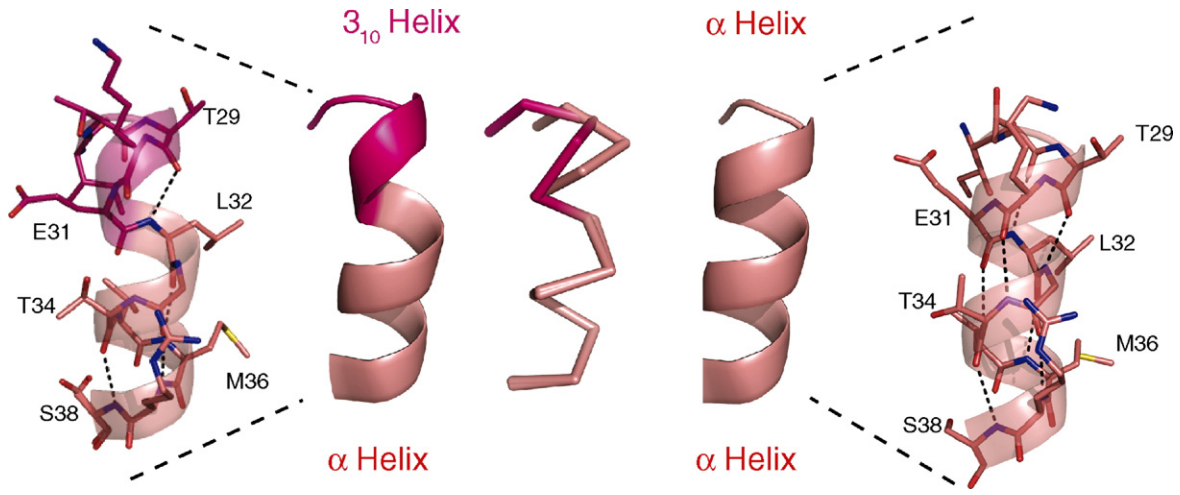

Fig. 5. Comparison of the N-terminal region of helix B of N-CaM (A) and Ca^{2+}-loaded CaM (1CLL). The segments of the helix that are in a traditional α-helical configuration are rose red, while the most N-terminal portion of the helix in our structure displays a 3_{10}-helical conformation and is magenta. The oxygen and nitrogen of residues are red and blue, respectively.

four-helix bundle changes N-CaM from a closed to an open conformation upon binding a metal ion.

Ca^{2+} regulates a diverse and vast number of cellular processes *via* transient increases from roughly 0.1 μM in a resting cell to 1–10 μM in an activated cell. However, the proteins largely responsible for primarily responding to this increase (CaM or other EF-hand proteins) accomplish this in the presence of 100- to 10,000-fold excess Mg^{2+} with very high selectivity for Ca^{2+}. The question of how EF-hand proteins are able to accomplish this remains one of the more intriguing aspects of this family of proteins, especially because it is thought that, in the absence of signaling or other events that produce large influxes of calcium, Mg^{2+} can at least partially populate EF-hand binding sites.[31,32] Through NMR shift experiments,[31–33] it has been postulated that Mg^{2+} can bind to the N-terminal portions of the N-CaM metal binding loops without inducing a conformational change. Interestingly, it was specifically shown that the bidentate glutamates in loop position 12 (Glu31 and Glu67) do not coordinate Mg^{2+} at all. In addition, the shift experiments conclude that Mg^{2+} only induces local conformational changes in and immediately around the binding loops, but does not induce the global conformational change from the closed to the open state as observed with Ca^{2+}. We also do not observe a large, global conformational change, although we do observe local shifts in conformation induced by Zn^{2+} binding. This may be related to the binding mode of these two divalent cations. In the EF-hand protein recoverin, the seven-coordinate Ca, Sr, Ba, and Cd divalent cations can induce large conformational changes, while the six-coordinate Mg cannot trigger a signaling response.

The specificity of EF-hand proteins for calcium has been proposed to depend on three things: the protonation state of the binding cavity, which gives rise to a preference for divalent cations; constrained cavity size as determined by specific side chains in the loop that have been referred to as "gatekeepers";[34,35] and the binding mode, referring here to the fact that calcium in proteins usually is 6–8 coordinated and prefers harder ligands (such as the oxygen atoms of carboxyl groups) and bidentate coordination.[36] As a divalent cation, zinc tends to prefer "softer" ligands (the sulfur atoms on cysteines or the nitrogen atoms on histidines). This is shown in its various coordination modes of the well-studied zinc finger family of structural proteins, involving 2Cys and 2His (cellular or transcription factor type zinc fingers), 3Cys and 1His (the retroviral type zinc fingers), or 4Cys (the steroid receptor type zinc finger). In zinc finger proteins and other enzymes, zinc is usually tetrahedrally coordinated, as we observe in our structure here. Interestingly, the harder ligand aspartates and glutamine are involved in our Zn^{2+}-bound N-CaM structure. This likely reflects the low affinity of such interactions, since a high concentration of Zn^{2+} ion is required to stabilize this crystal. Our structure can provide further evidence for the importance of the bidentate glutamate in position 12 because, in conjunction with the NMR shift studies proposing that Mg^{2+} can coordinate the N-terminal residues in the binding loop but not the bidentate glutamate, we also do not observe a large, global conformational change, although we do observe local shifts in conformation induced by Zn^{2+} binding. Our structure provides further knowledge of the structural basis for the conformational transition in CaM that is consistent with what we know about EF-hand protein metal ion coordination, calcium specificity, and transitional mechanism.

Materials and Methods

Protein expression and purification

N-terminal CaM was expressed from pProEx–N-CaM cloned from rat full-length CaM with a stop codon introduced after residue Lys78. This was transformed to a competent *Escherichia coli* BL21(DE3)pUBS520 strain and grown in 4 L of T7 LB medium at 30 °C overnight. Protein overexpression was induced by the addition of 0.2 mM IPTG when optical density at 595 nm reached 0.6–0.8. After overnight incubation, 0.1 M PMSF was added and cells were harvested by centrifugation (10,000 rpm for 10 min at 4 °C). Pellets were frozen and thawed before lysing with 0.1 mg/mL lysozyme lysis buffer, followed by sonication and ultracentrifugation to separate cell debris (35,000 rpm for 30 min). $CaCl_2$ (5 mM) was added to collected supernatants and this lysate was loaded onto a phenyl Sepharose column then eluted with 1 mM EGTA as described.[37] Peak fractions were collected, applied to a diethylaminoethyl column, and eluted with a salt gradient. Peak fractions as identified by SDS-PAGE were subjected to gel filtration (Superdex 75) and stored at −80 °C. This entire process was repeated for the purpose of growing selenomethionyl N-CaM, except that cultures were grown in minimal medium as described.[38]

Crystallization

Crystals of N-CaM and selenomethionyl N-CaM were grown using the hanging drop vapor diffusion method at 4 °C with reservoirs containing 1 mL of 100 mM sodium cacodylate, 5–10 mM zinc acetate, and 16% PEG8000. Crystals appeared after roughly 3 days and grew to a size of 400×500×100 μm over the course of 1 week. Crystals were frozen in liquid nitrogen cryosolutions containing 100 mM sodium cacodylate, 5–10 mM zinc acetate, 16% PEG8000, and 20% glycerol.

X-ray data collection, structure determination, and refinement

The structure was solved using single-wavelength anomalous diffraction data of the selenomethionyl-substituted protein. Data were collected at the Advanced Photon Source at Argonne National Laboratories (Argonne, IL). One complete data set representing peak parts of the selenium scattering spectrum was collected at 100 K at the radiation wavelength $\lambda_1 = 0.97929$ Å (peak). The data were processed with DENZO and scaled with SCALEPACK.[39] Six anomalous site positions were found by SOLVE,[40] including three Se, two Zn, and one As. The presence of these latter two metals was confirmed by

collecting data at the Zn and As edges and finding two and one anomalous sites, respectively. The structure was refined with SHARP.[41] The initial electron density map was obtained using the "remote" data set ($\lambda_3 = 0.97929$ Å). These experimentally obtained phases were then applied to a native N-CaM data set with very high resolution (approximately 1.3 Å) to generate a first model.

Segments of the model including individual helices were adjusted manually within the electron density map using the program Coot[42] followed by rigid body fitting with CNS. Side chains that had no clear representation in the electron density map were omitted from the model and the model was refined using the simulated annealing protocol in CNS.[43] After several cycles of manual model rebuilding, it became clear that additional electron density was present in one of the Zn^{2+}-binding sites. The extra density in site 1 could be modeled adequately with a cacodylate group that was present in the crystallization buffer. The cacodylate group coordinates and dictionary files for Refmac were built by CCP4.[44] After restrained and TLS refinements in Refmac reached values of $R_{work} = 0.146$ and $R_{free} = 0.192$, SHELX97 was used to include anisotropic refinement parameters. The quality of the structure was validated with the program PROCHECK.[45] Using this first model as a search model for the Ca^{2+}-soaked data set followed by a similar refinement protocol yielded $R_{work} = 0.138$ and $R_{free} = 0.190$. The model statistics are given in Table 1.

Adenylyl cyclase activity assay

Edema factor and adenylyl cyclase domain of CyaA were expressed and purified as previously described.[28,46] The activities of EF and CyaA were measured at 30 °C in the presence of 10 mM $MgCl_2$, 5 mM ATP, and a trace mount of [α-^{32}P]ATP for 10 min. The reaction was buffered by 50 mM Hepes (pH 7.2), and free calcium concentration was controlled by 10 mM EGTA to 1 μM based on calculations using the MAXC program. To test the activity of EF, 10 mM $ZnCl_2$ and 10 mM $MgCl_2$ were used. cAMP was separated from ATP by Dowex and alumina columns as described previously.[28] Initial velocities were linear with time and less than 10% of the ATP was consumed at the lowest substrate concentrations.

Protein Data Bank accession numbery

The atomic coordinates of Zn-trapped N-terminal CaM have been deposited in the RCSB Protein Data Bank with accession number 2PQ3.

Acknowledgements

We would like to thank the staff at the Advanced Photon Source, Argonne National Laboratories, for their expert advice and assistance in our data collection. Special thanks to Zenon Grabarek and Raymond Hulse for their critical reading of our manuscript and helpful comments. This work was supported by Grant GM62548 from the National Institutes of Health and a Howard Hughes Medical Institute Undergraduate Research Fellowship. Use of the Argonne National Laboratory Structural Biology Center and BioCARS beam lines at the Advanced Photon Source was supported by the U.S. Department of Energy, Office of Energy Research, under Contract W-31-109-ENG-38.

Supplementary Data

Supplementary data associated with this article can be found in the online version at doi:10.1016/j.jmb.2007.09.048

References

1. Means, A. R. (1988). Molecular mechanisms of action of calmodulin. *Recent Prog. Horm. Res.* **44**, 223–262.
2. Mandell, J. G., Roberts, V. A., Pique, M. E., Kotlovyi, V., Mitchell, J. C., Nelson, E. *et al.* (2001). Protein docking using continuum electrostatics and geometric fit. *Protein Eng.* **14**, 105–113.
3. Klee, C. B., Crouch, T. H. & Richman, P. G. (1980). Calmodulin. *Annu. Rev. Biochem.* **49**, 489–515.
4. Chin, D. & Means, A. R. (2000). Calmodulin: a prototypical calcium sensor. *Trends Cell Biol.* **10**, 322–328.
5. Xia, Z. & Storm, D. R. (2005). The role of calmodulin as a signal integrator for synaptic plasticity. *Nat. Rev. Neurosci.* **6**, 267–276.
6. Van Eldik, L. J. & Watterson, D. M. (1998). *Calmodulin and signal transduction,* Academic Press, San Diego.
7. Ishida, H. & Vogel, H. J. (2006). Protein–peptide interaction studies demonstrate the versatility of calmodulin target protein binding. *Protein Pept. Lett.* **13**, 455–465.
8. Schumacher, M. A., Crum, M. & Miller, M. C. (2004). Crystal structures of apocalmodulin and an apocalmodulin/SK potassium channel gating domain complex. *Structure*, **12**, 849–860.
9. Kuboniwa, H., Tjandra, N., Grzesiek, S., Ren, H., Klee, C. B. & Bax, A. (1995). Solution structure of calcium-free calmodulin. *Nat. Struct. Biol.* **2**, 768–776.
10. Finn, B. E., Evenas, J., Drakenberg, T., Waltho, J. P., Thulin, E. & Forsen, S. (1995). Calcium-induced structural changes and domain autonomy in calmodulin. *Nat. Struct. Biol.* **2**, 777–783.
11. Babu, Y. S., Bugg, C. E. & Cook, W. J. (1988). Structure of calmodulin refined at 2.2 A resolution. *J. Mol. Biol.* **204**, 191–204.
12. Babu, Y. S., Sack, J. S., Greenhough, T. J., Bugg, C. E., Means, A. R. & Cook, W. J. (1985). Three-dimensional structure of calmodulin. *Nature*, **315**, 37–40.
13. Chou, J. J., Li, S., Klee, C. B. & Bax, A. (2001). Solution structure of Ca(2+)-calmodulin reveals flexible hand-like properties of its domains. *Nat. Struct. Biol.* **8**, 990–997.
14. Grabarek, Z. (2005). Structure of a trapped intermediate of calmodulin: calcium regulation of EF-hand proteins from a new perspective. *J. Mol. Biol.* **346**, 1351–1366.
15. Akke, M. & Chazin, W. J. (2001). An open and shut case. *Nat. Struct. Biol.* **8**, 910–912.
16. Grabarek, Z. (2006). Structural basis for diversity of the EF-hand calcium-binding proteins. *J. Mol. Biol.* **359**, 509–525.
17. Guo, Q., Shen, Y., Lee, Y. S., Gibbs, C. S., Mrksich, M. & Tang, W. J. (2005). Structural basis for the interaction of *Bordetella pertussis* adenylyl cyclase toxin with calmodulin. *EMBO J.* **24**, 3190–3201.

18. Navaza, J. (1994). AmoRe: an automated package for molecular replacement. *Acta Crystallogr., Sect A: Found. Crystallogr.* **A50**, 157–163.
19. Rupp, B., Marshak, D. R. & Parkin, S. (1996). Crystallization and preliminary X-ray analysis of two new crystal forms of calmodulin. *Acta Crystallogr., Sect. D: Biol. Crystallogr.* **52**, 411–413.
20. Ishida, H., Takahashi, K., Nakashima, K., Kumaki, Y., Nakata, M., Hikichi, K. & Yazawa, M. (2000). Solution structures of the N-terminal domain of yeast calmodulin: Ca^{2+}-dependent conformational change and its functional implication. *Biochemistry*, **39**, 13660–13668.
21. Brunger, A. T., Adams, P. D., Clore, G. M., Delano, W. L., Gros, P., Grosse-Kunstleve, R. W. *et al.* (1998). Crystallography & NMR system: a new software suite for macromolecular structure determination. *Acta Crystallog. sect. D*, **54**, 905–921.
22. Chattopadhyaya, R., Meador, W. E., Means, A. R. & Quiocho, F. A. (1992). Calmodulin structure refined at 1.7 A resolution. *J. Mol. Biol.* **228**, 1177–1192.
23. Pedigo, S. & Shea, M. A. (1995). Quantitative endoproteinase GluC footprinting of cooperative Ca^{2+} binding to calmodulin: proteolytic susceptibility of E31 and E87 indicates interdomain interactions. *Biochemistry*, **34**, 1179–1196.
24. Beckingham, K. (1991). Use of site-directed mutations in the individual Ca2(+)-binding sites of calmodulin to examine Ca2(+)-induced conformational changes. *J. Biol. Chem.* **266**, 6027–6030.
25. Maune, J. F., Klee, C. B. & Beckingham, K. (1992). Ca^{2+} binding and conformational change in two series of point mutations to the individual Ca(2+)-binding sites of calmodulin. *J. Biol. Chem.* **267**, 5286–5295.
26. Baudier, J., Haglid, K., Haiech, J. & Gerard, D. (1983). Zinc ion binding to human brain calcium binding proteins, calmodulin and S100b protein. *Biochem. Biophys. Res. Commun.* **114**, 1138–1146.
27. Rainteau, D., Wolf, C. & Lavialle, F. (1989). Effects of calcium and calcium analogs on calmodulin: a Fourier transform infrared and electron spin resonance investigation. *Biochim. Biophys. Acta*, **1011**, 81–87.
28. Shen, Y., Lee, Y. S., Soelaiman, S., Bergson, P., Lu, D., Chen, A. *et al.* (2002). Physiological calcium concentrations regulate calmodulin binding and catalysis of adenylyl cyclase exotoxins. *EMBO J.* **21**, 6721–6732.
29. Shen, Y., Zhukovskaya, N. L., Guo, Q., Florian, J. & Tang, W. J. (2005). Calcium-independent calmodulin binding and two-metal-ion catalytic mechanism of anthrax edema factor. *EMBO J.* **24**, 929–941.
30. Nakashima, K., Ishida, H., Ohki, S. Y., Hikichi, K. & Yazawa, M. (1999). Calcium binding induces interaction between the N- and C-terminal domains of yeast calmodulin and modulates its overall conformation. *Biochemistry*, **38**, 98–104.
31. Malmendal, A., Evenas, J., Thulin, E., Gippert, G. P., Drakenberg, T. & Forsen, S. (1998). When size is important. Accommodation of magnesium in a calcium binding regulatory domain. *J. Biol. Chem.* **273**, 28994–29001.
32. Ohki, S., Ikura, M. & Zhang, M. (1997). Identification of Mg^{2+}-binding sites and the role of Mg^{2+} on target recognition by calmodulin. *Biochemistry*, **36**, 4309–4316.
33. Ohki, S., Miura, K., Saito, M., Nakashima, K., Maekawa, H., Yazawa, M. *et al.* (1996). Secondary structure and Ca(2+)-binding property of the N-terminal half domain of calmodulin from yeast *Saccharomyces cerevisiae* as studied by NMR. *J. Biochem. (Tokyo)*, **119**, 1045–1055.
34. Drake, S. K. & Falke, J. J. (1996). Kinetic tuning of the EF-hand calcium binding motif: the gateway residue independently adjusts (i) barrier height and (ii) equilibrium. *Biochemistry*, **35**, 1753–1760.
35. Drake, S. K., Zimmer, M. A., Kundrot, C. & Falke, J. J. (1997). Molecular tuning of an EF-hand-like calcium binding loop. Contributions of the coordinating side chain at loop position 3. *J. Gen. Physiol.* **110**, 173–184.
36. Dudev, T. & Lim, C. (2003). Principles governing Mg, Ca, and Zn binding and selectivity in proteins. *Chem. Rev.* **103**, 773–788.
37. Vogel, H. J., Lindahl, L. & Thulin, E. (1983). Calcium-dependent hydrophobic interaction chromatography of calmodulin, troponin C and their proteolytic fragments. *FEBS Lett.* **157**, 241–246.
38. Doublie, S. (1997). Preparation of selenomethionyl proteins for phase determination. *Methods in Enzymology*, **276**, 523–530.
39. Otwinowski, Z. & Minor, W. (1997). Processing of X-ray diffraction data collected in oscillation mode. *Methods Enzymol.* **276**, 307–326.
40. Terwilliger, T. C. & Berendzen, J. (1999). Automated MAD and MIR structure solution. *Acta Crystallogr., Sect. D: Biol. Crystallogr.* **55**, 849–861.
41. Bricogne, E. d. L. F. a. G. (1997). Maximum likelihood heavy-atom parameter refinement for multiple isomorphous replacement and multiwavelength diffraction methods. *Methods Enzymol.* **276**, 472–494.
42. Emsley, P. & Cowtan, K. (2004). Coot: model-building tools for molecular graphics. *Acta Crystallogr., Sect. D: Biol. Crystallogr.* **60**, 2126–2132.
43. Wilson, M. A. & Brunger, A. T. (2000). The 1.0 A crystal structure of Ca(2+)-bound calmodulin: an analysis of disorder and implications for functionally relevant plasticity. *J. Mol. Biol.* **301**, 1237–1256.
44. Collaborative Computational Project, Number 4. (1994). The CCP4 suite: programs for protein crystallography. *Acta Crystallogr., Sect. D: Biol. Crystallogr.* **50**, 760–763.
45. Laskowski, R. A., MacArthur, M. W., Moss, D. S. & Thornton, J. M. (1993). PROCHECK: a program to check the stereochemistry quality of protein structures. *J. Appl. Crystallogr.* **26**, 283–291.
46. Soelaiman, S., Wei, B. Q., Bergson, P., Lee, Y. S., Shen, Y., Mrksich, M. *et al.* (2003). Structure-based inhibitor discovery against adenylyl cyclase toxins from pathogenic bacteria that cause anthrax and whooping cough. *J. Biol. Chem.* **278**, 25990–25997.
47. Drohat, A. C., Amburgey, J. C., Abildgaard, F., Starich, M. R., Baldisseri, D. & Weber, D. J. (1996). Solution structure of rat apo-S100B(beta beta) as determined by NMR spectroscopy. *Biochemistry*, **35**, 11577–11588.